Global and Planetary Change 213 (2022) 103820

Contents lists available at ScienceDirect

Global and Planetary Change

journal homepage: www.elsevier.com/locate/gloplacha

The effect of climate change on wind-wave directional spectra

Hector Lobeto [a,*], Melisa Menendez [a], Iñigo J. Losada [a], Mark Hemer [b]

[a] IHCantabria - Instituto de Hidráulica Ambiental de la Universidad de Cantabria, Santander, Spain
[b] CSIRO Oceans and Atmosphere, Hobart, TAS, Australia

ARTICLE INFO

Editor: Dr. Howard Falcon-Lang

Keywords:
Wave spectrum
Wave climate
Climate Change

ABSTRACT

Through assessment of wind-wave directional spectra, we provide a comprehensive explanation of the projected 21st Century changes in the global wind-wave climatology under a high green-house emissions scenario. Using a seven-member wave climate projection ensemble, we estimate wave climate changes by comparing present and projected climatologies. Clustering techniques are applied to define regional patterns of change with homogeneous behavior. The underlying mechanisms behind the changes are also explored by exploiting the relationship between the wave generation area and the effective energy flux propagating toward a target location. A robust transition from positive to negative trends in Southern Ocean westerly swells is observed around 45°S. The increasing signal found in the southernmost swells propagates north beyond 30°N, contributing significantly to the projected changes in tropical regions such as the tropical southern Atlantic and tropical southeastern Pacific. Results highlight the great complexity of the Pacific Ocean due to the convergence of multiple wave systems with different geneses. In the northern basins, the combined effect of the ice melting and a poleward shift of the storm track drives an increase of the northernmost westerly swells. This is countered by a decreasing trend projected in the main wave systems propagating in the North Atlantic Ocean. A poleward shift of trade-induced waves due to the Hadley cell expansion can also be observed globally, causing a clear dipole change pattern in the tropical southern Atlantic and tropical Indian oceans.

1. Introduction

Wind waves are a key feature of the sea surface, with several co-existing wave trains of differing characteristics superimposed. At any point on the ocean surface, the wave climate is fully described as a stochastic process by the sea surface elevation spectrum. The spectral density variance captures contributions of superimposed wave fields characterized by different wave heights, periods and direction, depending on their relative point of origin. The variance spectrum, usually referred to as the energy spectrum as both variables are directly related (Holthuijsen, 2007), integrates the information about the genesis of the waves arriving at a specific location. In this regard, the shape, size and location of the peak from each local energy maximum within the spectrum relate to the geographical wave origin, maturity and amount of transported energy (Jiang and Mu, 2019). Despite the frequency-direction spectrum (hereinafter directional spectrum) being the most comprehensive way to describe the wave climate, it is common practice to use integrated wave parameters instead (e.g. significant wave height, wave period). The integrated wave parameters are defined from the sea surface elevation spectrum to provide an average representation of the wave conditions. Therefore, its definition implies the loss of information about the multimodality of the sea state (i.e. number of wave systems propagating at the same time) and the actual relation between the different variables included in the spectrum (i.e. energy, period and direction). The inclusion of wave climate information in coastal engineering formulations such as in coastal structure design or in coastal processes modeling (e.g. Usace, 1984) is typically captured through integrated parameters, but this can lead to an over-simplification of the wave-field (Lobeto et al., 2021b).

The use of directional spectra to develop climate studies is still limited. The availability of full spectra from real measurements is both recent and scarce. There is a growing but still low number of spectral buoys available with a heterogenous spatial coverage, precluding development of large-scale studies. In the same vein, satellite altimetry is yet progressing on providing a global database of wave spectra. Therefore, the use of directional spectra is mainly limited to the products of numerical simulations and conditioned by the relatively high data storage requirements for high frequency (e.g., hourly) spectra.

* Corresponding author.
E-mail address: lobetoh@unican.es (H. Lobeto).

https://doi.org/10.1016/j.gloplacha.2022.103820
Received 9 November 2021; Received in revised form 2 March 2022; Accepted 14 April 2022
Available online 25 April 2022

Typically, discrete wave-model spectra store of order 500–1000 values per archived time-step, which is a significant cost relative to storing several integrated parameters at the same temporal frequency. The great complexity inherent to its multidimensionality is a further reason behind the low usage of full spectral information. However, the analysis of directional spectra has already led to a very detailed description of the wave climate in some regions, such as the North Sea (Boukhanovsky et al., 2007), the coast of Spain (Espejo et al., 2014) or the coast of Japan (Shimura and Mori, 2019). More recently, the wave spectral modality has been assessed at global scale, also determining its seasonality (Echevarria et al., 2019). Furthermore, the relation between these wave modes and different teleconnection patterns can also be analyzed, shedding light on the drivers of the inter-annual wave variability (Echevarria et al., 2020). In addition, as the directional spectrum contains information about the convergent wave systems, different methods have been proposed to isolate each of them (Portilla et al., 2009). Then, the derived product can be statistically analyzed (Portilla-Yandún et al., 2019, 2015) to determine the frequency, age and wave height associated to each wave system as has been done globally in the GLOSWAC database (Portilla-Yandún, 2018).

The effect of climate change on surface wind waves has been a recurrent subject of study during the last two decades. In this regard, the COWCLIP community (Coordinated Ocean Wave Climate Project) integrates efforts to reunite the existent studies on the matter and to offer an estimation of the uncertainty associated with observed historical and projected future changes (Morim et al., 2018, 2019, 2020). The development of atmosphere-ocean circulation models (GCMs) has provided the resources to build wave climate projections and to study the future wave conditions under different green-house gas emission scenarios and time horizons. GCMs reproduce the real global climate, representing the physical processes in the atmosphere, ocean, cryosphere and land, as well as their complex interactions (Flato et al., 2013). Nevertheless, certain issues such as the parametrizations included in the models to reproduce some physical processes or the spatial resolution cause intrinsic biases (Maraun et al., 2017). These biases are inevitably transferred to the wave model forcings (i.e. marine surface wind fields) and therefore to the wave climate (Hemer et al., 2012). A reliable study of the future behavior of wind waves necessarily needs to be held by a realistic representation of the wave climate, although always being aware of the limitations of the data used to develop the analysis. Concerning the latter, despite bias correction (BC) allowing more accurate results in the simulated wave climate to be obtained, and assumed to carry to the projected changes in integrated parameters (Lemos et al., 2020), a direct extrapolation of the commonly used correcting methods to directional spectra cannot be done.

Two are the main approaches used to generate wave climate projections from GCMs forcings: statistical and dynamical. Although statistical projections have been a helpful way to obtain future wave series without a massive computational demand (e.g., P. Camus et al., 2017; Perez et al., 2015; X. L. Wang et al., 2014), many studies now use dynamical simulations to investigate potential changes (e.g., Fan et al., 2013; Hemer et al., 2013; Mori et al., 2013; Semedo et al., 2013). The projected changes are commonly estimated from the outputs of wave climate projection ensembles. Thus, the uncertainty associated with the change signal of each GCM is partly overcome through the assessment of the ensemble mean change, which normally implies the evaluation of the agreement between members and/or the statistical significance of the estimated variation (Collins et al., 2013).

The standard approach to assess the future behavior of wave conditions consists in analyzing the projected changes in integrated wave parameters (e.g. significant wave height, mean wave period or mean wave direction). In particular, the significant wave height (H_s) has been the most studied parameter as its changes are considered a representation of the expected variations in the energy captured in the full spectrum. The assessment of changes in wave period (e.g. Casas-Prat et al., 2018) or in variables that integrate both the wave height and period, such as wave energy flux, is gaining popularity (Lemos et al., 2019; Mentaschi et al., 2017; Reguero et al., 2019). This fact demonstrates the advances of the climate community in having a broader understanding of the effect of climate change on ocean wind waves, not being constrained to the limitations offered by the analysis of only H_s. For completeness, the proven influence of the wave characteristics in future projected coastal processes like shoreline evolution (Alvarez-Cuesta et al., 2021b, 2021a; Toimil et al., 2021), provides a compelling reason to expand the assessment to less analyzed wave parameters (e.g. period, direction), yet acknowledging there is higher uncertainty in these (Morim et al., 2019). More recently, new studies based on the analysis of each independent wave system through its associated H_s have been developed (Amores and Marcos, 2020; Fan et al., 2014; Lemos et al., 2021b). Although these analyses are not based on spectral data but derived from integrated parameters using swell-tracking formulation, they have demonstrated the existence of different climate change signals for different systems and the importance of directionality. On this basis, Lobeto et al., 2021b proposed an approach to assess the projected change in wave climate due to climate change based on the use of directional spectra, discussing its added-value with respect to the use of integrated parameters. According to the results presented, integrated parameters can mask valuable information concerning the sign, magnitude and robustness of the actual change. The presence of wave systems within the spectrum with an associated change of opposite sign can induce misleading results when applying the standard approach due to the offset of positive and negative variations. However, the limited number of locations analyzed in the mentioned study precluded conclusions about the expected change in swell systems at global scale.

The present study intends to go further, contributing to the understanding of the future behavior of wind waves globally through the assessment of the projected changes in wave energy from directional spectra. The scope is not only limited to provide a global overview of the projected changes, but also to identify regional patterns of change to describe the future behavior of the main wave systems propagating across the oceans.

The Manuscript is organized as follows: Section 1 describes the wave climate data used and Section 2 all the methods applied. Section 3 summarizes the main results obtained in this study. Finally, the main conclusions derived from the research are included and discussed in Section 4.

Table 1
Main characteristics of the Atmosphere-Ocean General Circulation Models considered for this study.

GCM	Institution	Country	Atmospheric resolution (lat x lon)
MIROC5	MIROC	Japan	1,40° x 1,40°
IPSL-CM5A-MR	Institut Pierre-Simon Laplace	France	1,25° x 1,25°
GFDL-ESM2G	NOAA Geophysical Fluid Dynamics Laboratory	USA	2,00° x 2,50°
CNRM-CM5	Centre National de Recherches Météorologiques	France	1,40° x 1,40°
CMCC-CM	Centro Euro-Mediterraneo per I Cambiamenti Climatici	Italy	0,75° x 0,75°
ACCESS1.0	CSIRO-BOM	Australia	1,25° x 1,90°
HadGEM2-ES	Met Office Hadley Centre	UK	1,25° x 1,90°

2. Wave climate data

The effect of climate change on wave climate is studied through the outputs of a seven-member wave climate projection ensemble dynamically simulated with the third-generation numerical wave model WaveWatchIII v4.18 (Tolman, 2014). The model forcings are surface wind fields and ice coverage outputs from seven atmosphere-ocean general circulation models (GCMs). The GCMs are selected on the

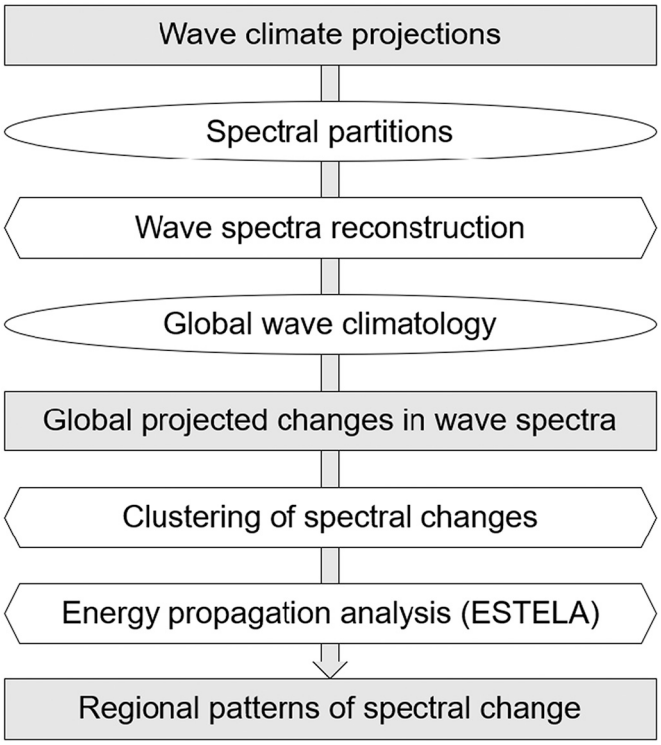

Fig. 1. Scheme overview of the methodology. Rectangles represent main results, ellipses intermediate results and hexagons methods.

basis of the highest possible time resolution, all of them providing 3-hourly wind and daily ice fields (with the only exception of HadGEM-ES with monthly ice). Table 1 summarizes the main characteristics of the GCMs considered (further details can be found at *https://esgf-node.llnl.gov/projects/cmip5/*, last time accessed on November 2021). Present-day and future wind-wave climate are simulated through the twenty-year time slices 1986–2005 and 2081–2100, respectively. The projected wave conditions are modeled under the RCP8.5 green-house gas (GHG) emission scenario stated in the Fifth Assessment Report from IPCC (AR5, Cubasch et al., 2013). It represents a concentration trajectory characterized by a radiative forcing of 8.5 W/m^2 by 2100 in the absence of a drastic reduction of GHG emission rates. In addition, a simulation for the historical period with forcings from ERA5 and the very same numerical model configuration as for the GCM-driven wave simulations is developed to be used as reference data.

The simulations are run in a regular near-global mesh covering latitudes between 88°N and 85°S with one-degree spatial resolution. A continuous ice treatment from an ice coverage of 25% (no obstruction) to 75% (complete obstruction) is considered. Below 25% no wave energy dissipation is assumed, whereas a sea ice coverage above 75% is assumed to cause a complete dissipation of energy. As a result, we store hourly time series of integrated wave parameters and spectral data. The storage of full directional spectra at hourly resolution requires large capacity resources, even more considering the number of GCMs used and the global perspective of the study. Hence, we implement an alternative approach to reconstruct the directional spectra based on the use of spectral partitions. A spectral partition (SP) represents each of the wave systems reaching a certain location at any time and can be identified as each of the spectral peaks within the full spectrum (Portilla-Yandún et al., 2015). The isolation of each SP and its treatment as an independent spectrum enables to calculate their associated integrated wave parameters (hereinafter spectral partition parameters, SPP). The number of SP varies in time and space, influenced by the climate variability at different scales (e.g. seasonal, interannual) and the exposure of the target location to the open ocean (i.e. the possibility of being reached by multiple wave systems propagating from different directions), among other factors. In general, the wave climate is dominated by one or two swell systems, although additional secondary systems can also exist. For example, according to the study of Echevarria et al. (2019), while a location in the northeastern Atlantic is mostly affected by one swell system, locations in the tropical Pacific can be affected by five different swell systems. Considering so, the number of SP stored is a compromise between an accurate reconstruction of full spectra from hourly time series of SPP and a reasonable amount of data to be stored. Here, three SP are used, two of them corresponding to swell systems and the remaining related to wind sea waves. The spectral partitioning scheme used in the propagation numerical model is based on an analogy between the surface-elevation spectrum and a topographic surface (Hanson and Phillips, 2001). In this context, the sub-peaks and associated surface are identified by applying a digital image watershed partitioning algorithm, implemented as described in Tracy et al. (2007). For each SP the parameters significant wave height (H_s), peak period (T_p), mean direction (Dir_m) and directional spread (Spr) are stored.

3. Methods

3.1. Methodology overview

Fig. 1 shows a flowchart summarizing the approach followed in this study. The methodology is based on a seven-member wave climate projection ensemble. As a result of the simulations, a global spectral dataset of three spectral partitions is produced. Next, spectra are reconstructed from the partitional information globally at 8-degree spatial resolution. Projected changes in wave climate are then estimated by comparing present and future mean climatologies. Resulting annual mean changes are geographically classified into sixteen ocean regions with a similar pattern of spectral change using a K-means algorithm. Finally, the underlying mechanisms behind the changes found in the wave systems are explored using the ESTELA method (Pérez et al., 2014).

3.2. Spectral reconstruction

The reconstruction of directional spectra from SPP (i.e. H_s, T_p, Dir_m, Spr) needs to be grounded on a theoretical basis to define the spectral partition shape. We consider the JONSWAP (Joint North Sea Wave Project) spectrum (Hasselmann et al., 1973) due to its extended use in multiple studies related to coastal and ocean engineering (Benoit, 1992; Onorato et al., 2001; Rueda-bayona et al., 2020; Y. Wang, 2014; Whittaker et al., 2016). The generation conditions of the observed waves used to define the formulation initially restrict its validity for developing seas with a limited generation fetch. However, over the years the JONSWAP spectrum has been proven to be valid for a wider range of wave generation conditions, including storms and hurricanes, making it the most extended design spectrum for coastal engineers (Holthuijsen, 2007).

Among the multiple formulas derived from the original JONSWAP research (e.g. Donelan et al., 1985; Goda, 2010), we use the one proposed by Goda. This expression considers the spectral shape in terms of the significant wave height and peak period of the sea state and three calibration parameters: β_j is the energy scale parameter, σ is the peak-width parameter and γ is the peak-enhancement parameter. The peak enhancement parameter varies through time depending on the transported energy and degree of development of the sea state, i.e. it takes higher values for mature frequency-filtered swells and energetic sea states. Here, we use an average γ of 3.3, which is the standard approach among the coastal engineering community (Holthuijsen, 2007). Similarly, we consider the average values $\sigma_a = 0.07$ and $\sigma_b = 0.09$ for the peak-width parameters (Hasselmann et al., 1973).

Since we are reconstructing directional spectra, a correct representation of the real spectrum entails defining as accurately as possible the

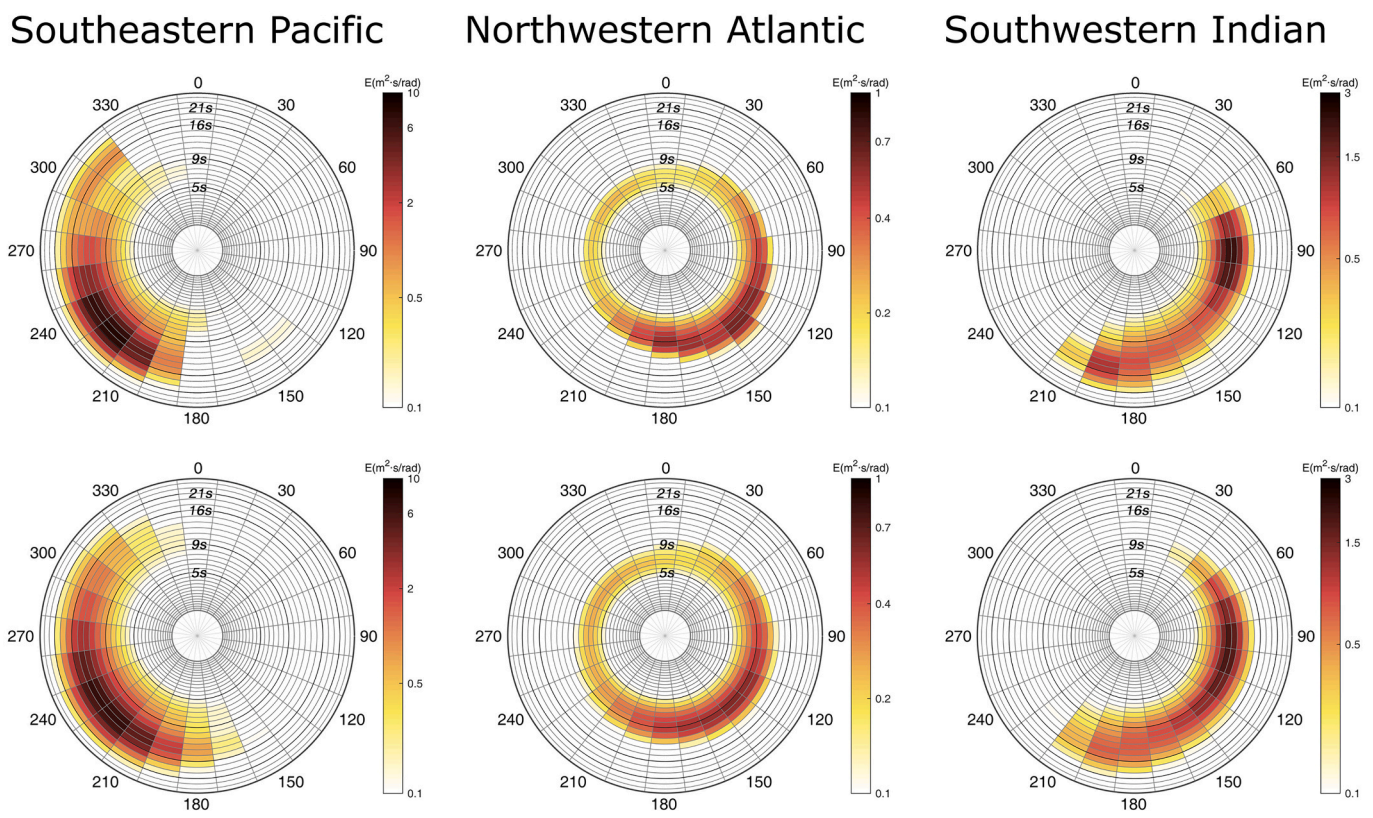

Fig. 2. Annual mean wave energy for the period 1986–2005 and CMCC-CM model from full directional spectra (upper panels) and reconstructed directional spectra (lower panels) at three locations from different ocean basins.

energy spreading across directional sectors. Among the different directional spreading functions proposed in the literature (e.g. Longuet-Higgins et al., 1963; Pierson Jr. et al., 1952), the Mitsuyasu et al. (1975) formulation is selected to this purpose. This function assumes a decay in the energy from its maximum at the principal wave direction until zero for an azimuth equal or greater than 180°.

The reconstruction scheme of the full directional spectrum defines the spectral shape for each partition as a JONSWAP spectrum. Then, the directional spreading coefficient is calculated for each direction to scale the spectral shape. Finally, the full directional spectrum is obtained as the sum of all the reconstructed partitions. In this study, the spectral wave energy is discretized in 32 frequency bins, exponentially distributed from 0.0373 to 0.7159 Hz (i.e., from 1.4 to 26.8 s) and 24 directional sectors of 15° each, i.e., each spectrum is divided into 768 frequency-direction spectral bins (hereinafter spectral bins). We analyze spectral conditions globally at 8-degree spatial resolution,

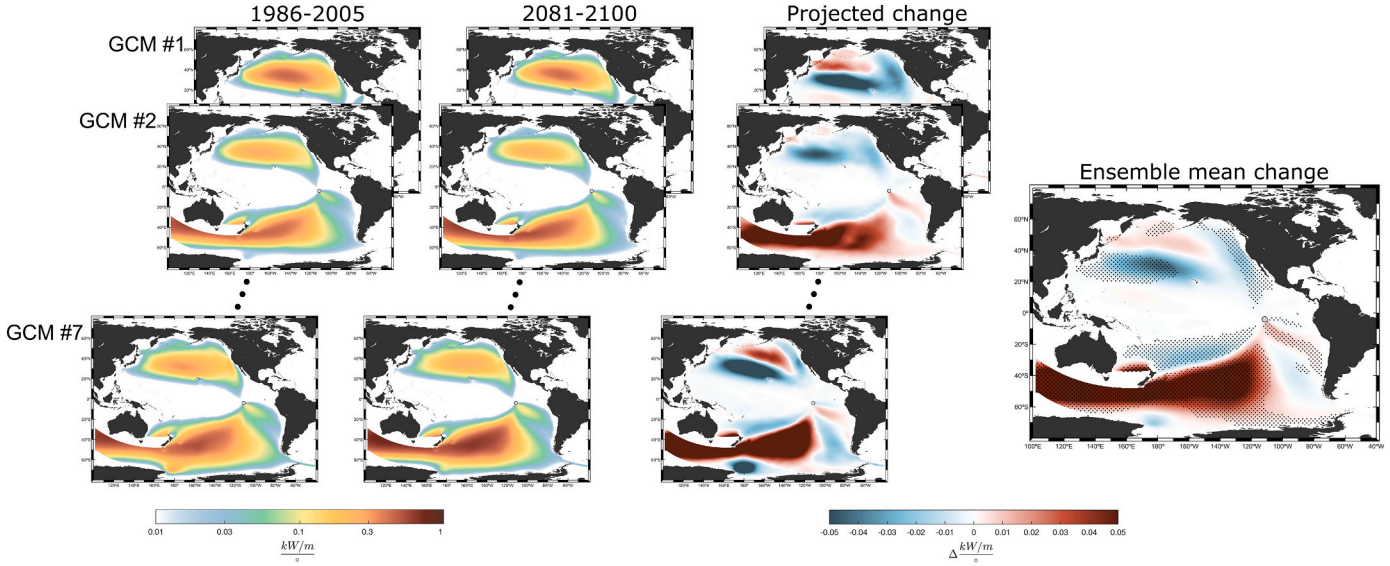

Fig. 3. Assessment scheme of the projected changes in effective energy flux propagating toward a target location. Left panels: Present-day and projected mean effective energy flux. Central panels: Projected change in mean effective energy flux. Right panel: Ensemble mean projected change in mean effective energy flux. Stippling indicates robust projected changes.

resulting in a total of 491 spectra.

The reconstruction is validated by comparison with full directional spectra equally discretized (i.e. 24 directions, 32 frequencies). Fig. 2 shows the result of the reconstruction in three locations from different basins and for the CMCC-CM climate member. The first one is located in the southeastern Pacific (37°S, 74°E), the second one in the northwestern Atlantic (40°N, 73°W) and the third one is located in the southwestern Indian (18°S, 50°E). The validation evidences a good representation of the annual mean climatology by the reconstructed spectra. A slight overestimation of the total energy in the reconstructed spectra is however observed. This overestimation is 4%, 7% and 3% for the SE Pacific, NW Atlantic and SW Indian spectra, respectively. The energy spread across directional sectors and frequencies is also well captured. For each of the three spectra showed in Fig. 2, the mean relative error in the energy proportion at each 15-degree directional sector is 12%, 8% and 16%, and at each of the 32 frequency bins is 7%, 5% and 13%, respectively. For a given set of bins, the mean relative errors are calculated as the mean of the absolute normalized differences in the proportion of energy between the full and the reconstructed spectra.

3.3. ESTELA method

The ESTELA method (Pérez et al., 2014) allows to study the propagation of the wave energy from the generation area to any ocean location assuming that it travels along great circle paths (Young, 1999). It provides valuable information about the genesis of the waves, unraveling where they were generated and the different energy contribution among ocean regions. Furthermore, the analysis of the energy flux and its variations along the great circle paths determines not only the travelling time of the waves to reach the analyzed point, but also the main areas of energy gain and dissipation. Here, the ESTELA method complements the analysis of directional spectra, helping to define the generation area of the different wave systems discernible within the spectrum and their projected changes under climate change scenarios.

The effective energy flux (EF_w) propagating toward a target location from any ocean point is calculated based on geographical and physical criteria. The obstacles encountered by the wave trajectory, such as islands or mainland, determines firstly whether the energy can travel from a point to another. Then, the EF_w at each ocean point is obtained as the portion of energy heading the target location along the circle path. The total energy is calculated following the same spectral reconstruction method previously explained. Thus, the spreading function determines the fraction of the total that propagates toward the direction of analysis.

The annual mean EF_w is calculated for the present-day and future time slices at the points of interest for all the ensemble members. Then, the ensemble mean projected change in annual mean EF_w is estimated and the associated uncertainty is assessed. Fig. 3 shows an example for a point located in the tropical eastern Pacific Ocean.

3.4. Projected changes and uncertainty assessment

We assess the differences between the present-day and projected end of the century wave climate under the high emission scenario RCP8.5. The projected change is estimated as the unweighted ensemble mean change, i.e. it is calculated as the average of the individual changes from each member assuming a homogenous contribution from all of them.

The proposed method to assess the uncertainty of the projected changes is based on one of the techniques proposed in AR5 (Collins et al., 2013). The robustness of the future variations at each frequency-direction bin is evaluated in terms of the individual statistical significance of the change for each model and the homogeneity of the sign of change between the members of the ensemble. Therefore, the change is considered robust when more than 80% of the members present a statistically significant change at 95% confidence level and at least 80% of those agree in sign of change. The statistical significance is calculated by applying a Welch's *t*-test to the mean of the historical and future periods at 95% confidence level (Tebaldi et al., 2011). The implementation of a heteroscedastic t-test is based on the possible shift of the energy from present-day to future periods, thus precluding to assume an equal variance at each spectral bin. Spectral bins showing robust changes are stippled. We do not consider changes lower than a 1% the maximum variation within the spectrum, to avoid noise in the representation of the results. The projected changes in H_s are also assessed as described above. The projected changes in EF_w are considered as robust when the absolute value of the change is higher than the inter-model standard deviation.

3.5. Clustering

The projected changes in annual mean spectral energy are clustered to identify ocean regions with a similar change pattern. Numerous unsupervised machine learning techniques to perform data clustering can be found in the literature (e.g. k-means, DBSCAN, spectral clustering). The main feature of these algorithms is that they are able to group the observations without being trained before with labeled data. They are classified in terms of the set of rules they follow to assess the similarity between observations. An intuitive classification is to divide the algorithms between partitioning and hierarchical methods (Kaufman and Rousseeuw, 2009). After testing several clustering techniques, we select k-means (Lloyd, 1982) due to its simplicity and its proven suitability to develop wave climate studies (e.g. Camus et al., 2011, Camus et al., 2014; Lucio et al., 2020).

K-means is based on the minimization of the distance between the center of mass of each cluster and its members. Thus, from a given k number of clusters and n observations $x_1, x_2, \ldots, x_n$, the algorithm finds the centers c so as to minimize a potential function. The potential function varies depending on the distance metric considered (e.g. Euclidean, cosine). In this particular case, we use the squared-Euclidean distance. The initialization plays a key role in the performance of the algorithm in terms of speed and accuracy (Arthur and Vassilvitskii, 2007). In this regard, Lloyd's algorithm proposes a random selection of the initial centroids, which implies that results could be different on each realization. To avoid this source of uncertainty, the initial centers are selected using the maximum dissimilarity algorithm (Snarey et al., 1997).

K-means is applied to the spectral changes considering the spectral bins as variables and the spectra as observations, i.e. 768 variables with 491 observations each. The high number of variables and analyzed locations requires a preprocessing to assist the clustering algorithm and remove noisy signals. First, the input dimensionality is reduced by aggregating the spectral bins, changing from the initial discretization of 24 directions and 32 frequencies to 12 and 5, respectively. The aggregation is done so that each new spectral bin represents a directional sector of 30° and the following period ranges: <5 s; 5 s – 10s; 10s – 15 s; 15 s – 20s; >20s. Then, the variable of analysis is transformed by applying the function $Y = X^{1/3}$ to reduce the variance between spectral bins. Finally, we apply principal component analysis in the sample of variables and observations, considering only the principal components that explain 99% of the variance. We apply the clustering to the Atlantic, Pacific and Indian oceans independently. The final number of clusters for each basin is selected iteratively, on the basis of the minimum number that can represent the spatial change pattern variability.

4. Results

Prior to the assessment of projected changes, the biases in spectral energy and H_s relative to the reference hindcast are analyzed to evaluate the skill of the ensemble members to reproduce the wind-wave climatology (Supplementary Fig. 1). Results show that, in agreement with previous studies (Lobeto et al., 2021b), the bias of the spectral energy can vary not only from one member to another, but also within the

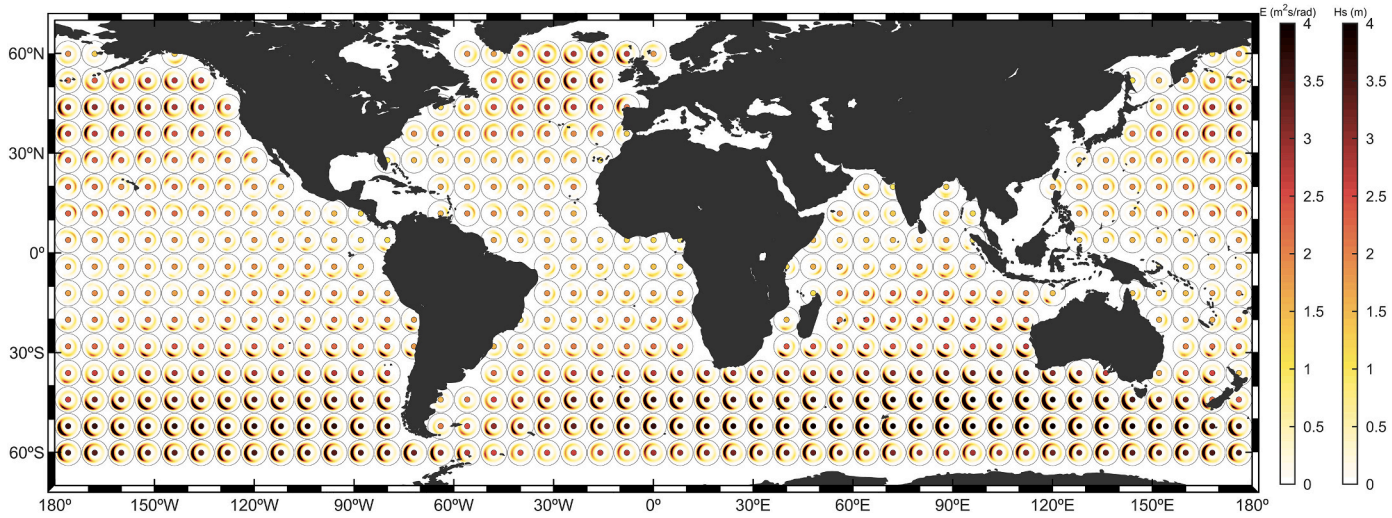

Fig. 4. Annual mean wave climate estimated for the period 1986–2005 and the ensemble mean. The map displays the annual mean wave spectral energy (polar plot) and the annual mean significant wave height (dots in the center of the polar plots).

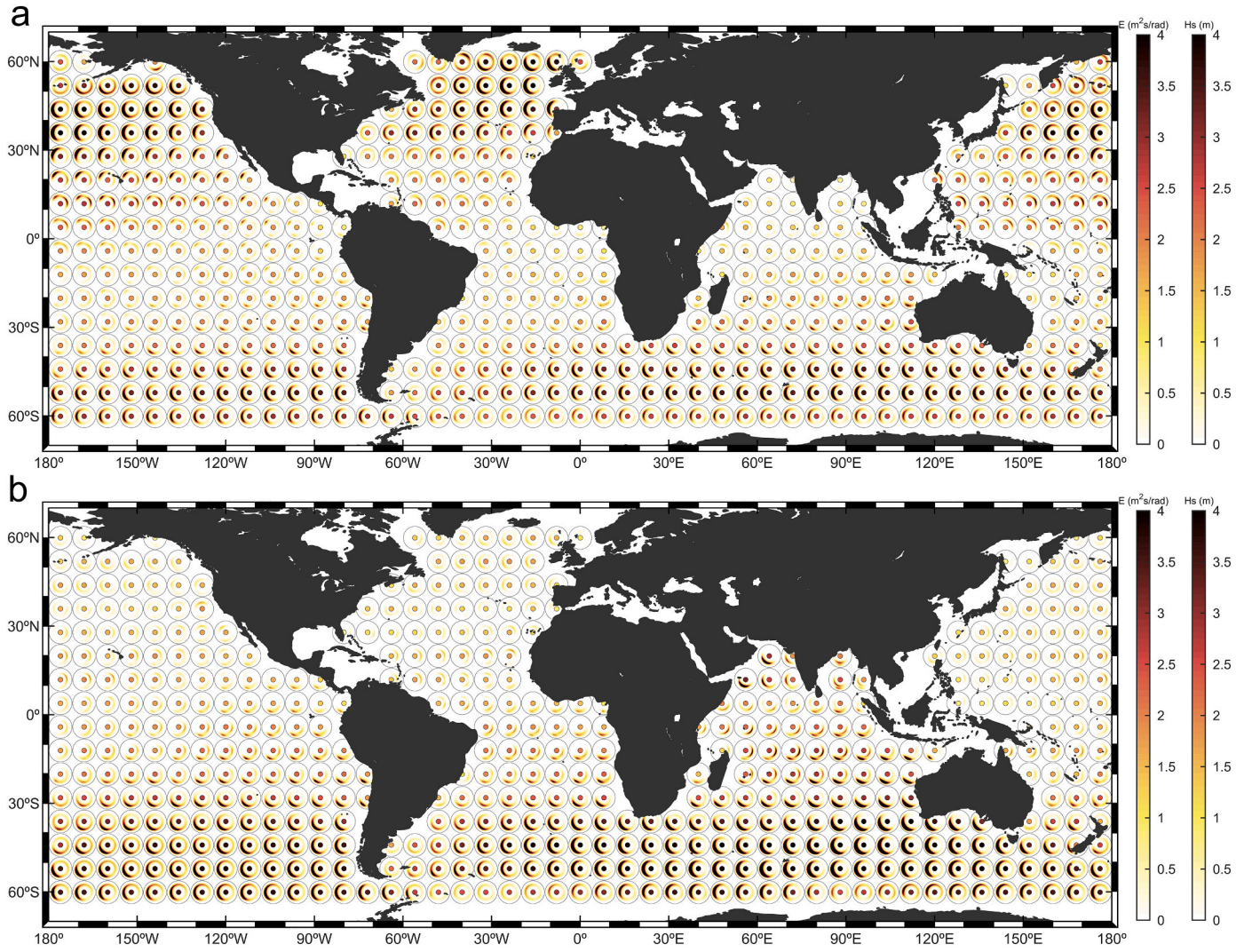

Fig. 5. (a) Boreal winter (DJF) and (b) boreal summer (JJA) mean wave climate estimated for the period 1986–2005 and the ensemble mean. The maps display the seasonal mean wave spectral energy (polar plot) and the seasonal mean significant wave height (dots in the center of the polar plots).

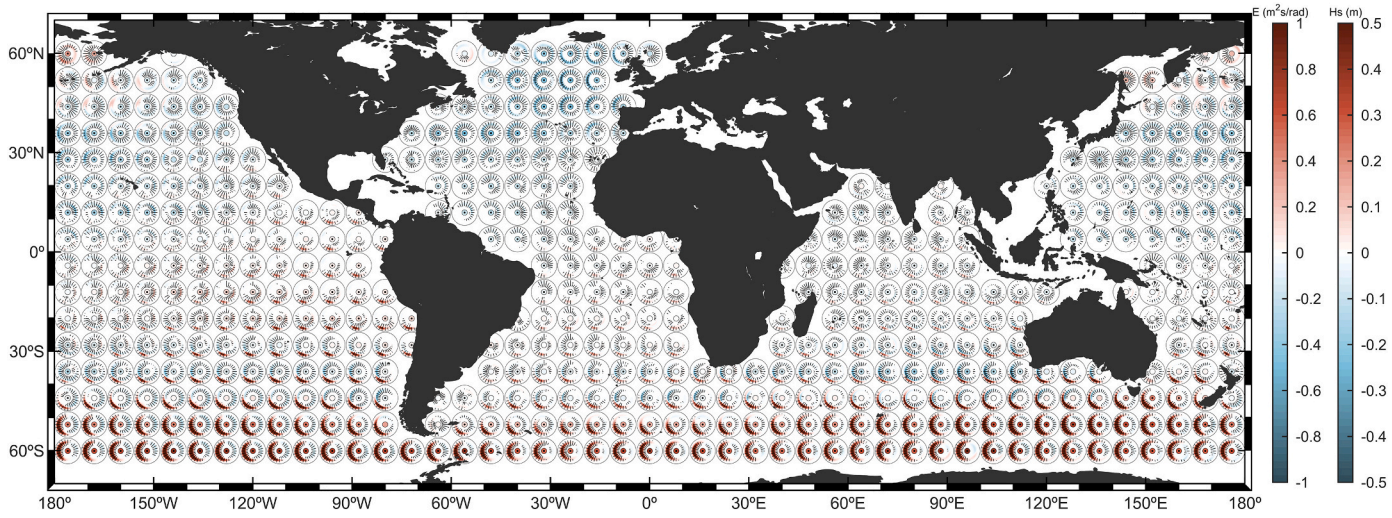

Fig. 6. Ensemble mean projected changes in annual mean wave spectral energy (polar plots) and significant wave height (dots in the center of the polar plots). Stippling indicates robust projected changes.

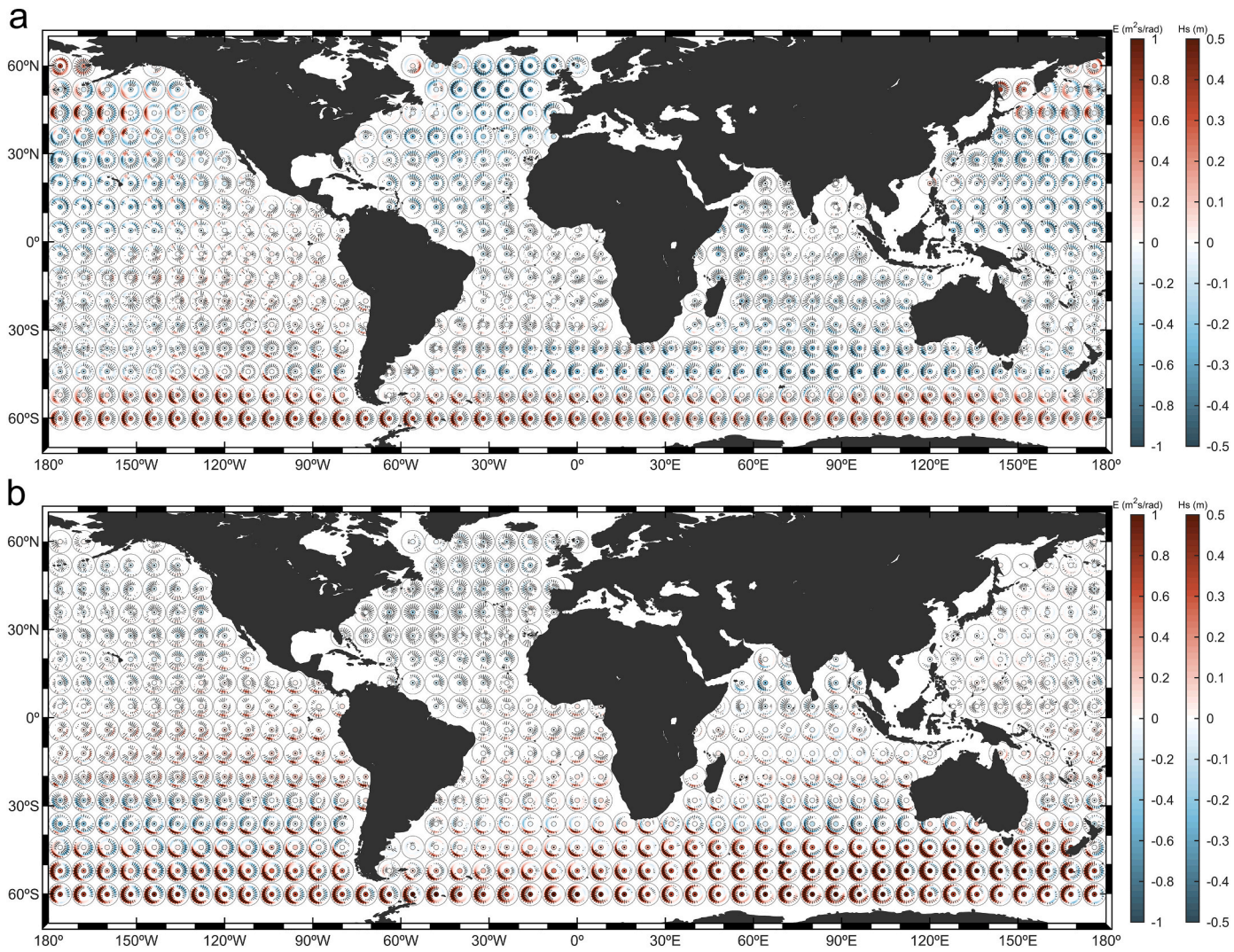

Fig. 7. (a) Ensemble mean projected changes in boreal winter (DJF) and (b) boreal summer (JJA) mean wave spectral energy (polar plots) and significant wave height (dots in the center of the polar plots). Stippling indicates robust projected changes.

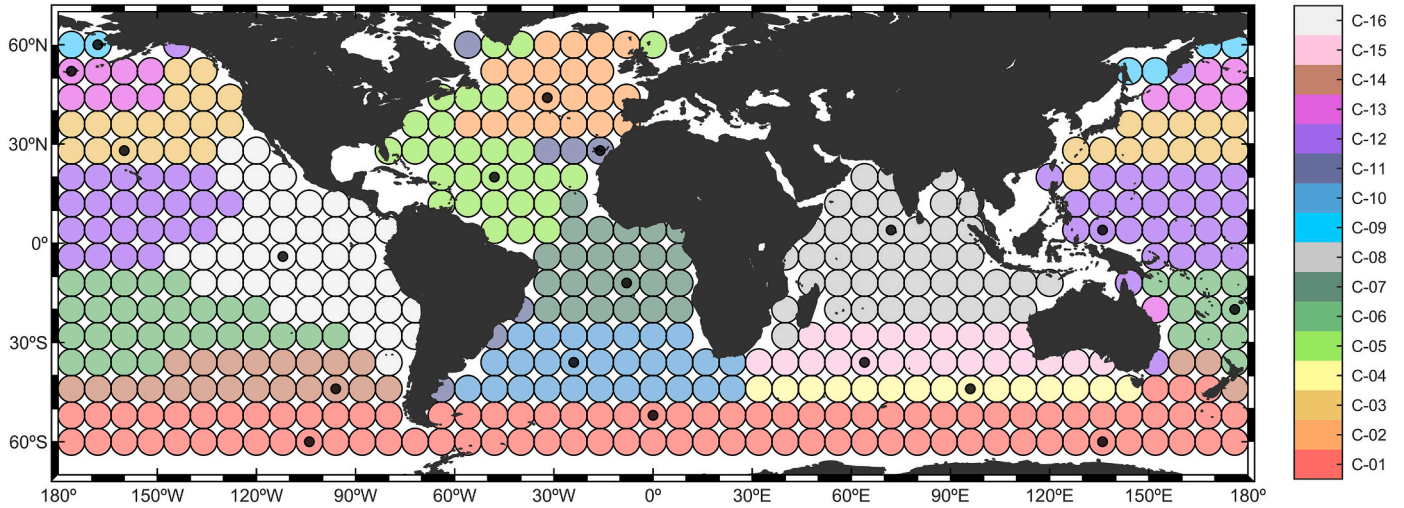

Fig. 8. Sixteen regional patterns of spectral change. Black dots indicate the reference location used to analyze each cluster.

spectrum, i.e. wave systems can show biases with different magnitude and sign. While CMCC-CM and MIROC5 mostly overestimate the present-day H_s climate, the rest of the models show a general underestimation. ACCESS1.0 and GFDL-ESM2G are the models that show the lowest biases, presenting a global mean bias in H_s of −0.07 m and − 0.14 m, respectively. CNRM-CM5 and IPSL-CM5A-MR show the greatest discrepancies (−0.29 m and − 0.48 m, respectively). These results, although taken with caution, provide confidence in the wave climatology representation and the estimated projected changes from the GCM-based wave spectral data.

In view of the above, the annual (Fig. 4) and seasonal (Fig. 5 for DJF and JJA; Supplementary Fig. 2 for MAM and SON) mean wave climatology for the historical period is analyzed from the ensemble mean. There is high dominance of extra-tropical swells across the global ocean as they transport most of the wave energy. These swells mainly propagate from the west across the extra-tropical regions (Odériz et al., 2021), showing a clear seasonal change pattern characterized by more energetic swells during the winter season. The Southern Ocean (SO) is the most energetic ocean basin, favored by the long continuous fetch south of 40°S, only partially interrupted by the southernmost part of America (Semedo et al., 2011; Young, 1999). Seasonal mean climatology shows very energetic westerly swells in the SO regardless the season analyzed, which are notably strong in the Indian region during the austral winter. The seasonality is more prominent in the Northern Hemisphere, showing big differences between the energy transported by westerly swells during winter and summer seasons.

The extra-tropical swell systems also propagate toward the equator, converging with less-energetic easterly wave systems generated in the tropical region by the trade winds. Thus, tropical and extra-tropical wave systems coexist in all ocean basins between 30°S and 30°N and especially in the Pacific, which agrees with the results shown by Echevarria et al. (2019). As a result, the dominant system in the north tropical region varies seasonally depending on the extra-tropical swell contribution. Although weak seasonal patterns can also be observed in swells induced by trade winds, except for the Monsoon areas where it is more prominent (Dima and Wallace, 2003), there is a change from an almost even contribution from extra-tropical and tropical swells during the winter season to a clear dominance of the latter during the summer. The areas affected by the Monsoon phenomenon in the northwestern Indian Ocean show remarkable seasonal differences. In this regard and consistent with previous studies (Portilla-Yandún, 2018), the Monsoon-induced winds generate waves that propagate from the northeast during the boreal winter and from the southwest during summer.

We compare the mean wave climatology for the historical and future periods and every ensemble member, subsequently estimating the ensemble mean projected changes in both the spectral energy and H_s parameter. The changes in annual mean wave energy are shown in Fig. 6. Seasonal changes are depicted in Fig. 7 for DFJ and JJA and in Supplementary Fig. 3 for MAM and SON. The projected changes in annual mean spectral energy show a robust projected increase in westerly swells generated in the SO, which is consistent with the community consensus about the projected increase in H_s in this region (e.g. Morim et al., 2018; Oppenheimer et al., 2019). The increasing change signal propagates north across all ocean basins, reaching latitudes beyond 30°N in the Pacific and Atlantic oceans, mainly during the austral winter season. The projected increase in SO swells dominates not only the projected changes in H_s in the SO, but also significantly contributes to the change expected in tropical areas. For example, there exists agreement on a projected increase in H_s in the tropical southeastern Pacific that is mainly attributed to the expected increase in the intensity of southeasterly Pacific trades (e.g. Hemer et al., 2013; Lobeto et al., 2021a). However, the spectral analysis indicates that the energy increase in this region is also affected by the increase in swell energy from the SO, especially in the easternmost area. Results also show a northward transition from positive to negative changes in SO westerly wave energy in every basin, which agrees with previous studies (Fan et al., 2014). Moreover, this boundary seasonally shifts, moving north during the austral winter and the opposite during the summer.

Results show a robust projected decrease in swells generated in the extra-tropical North Atlantic Ocean. The decreasing signal propagates south, combining in the tropical region with the decreases expected in waves generated by northeasterly trade winds. Thus, there is a projected decrease in the whole North Atlantic basin consistent with the community agreement (Morim et al., 2018; Oppenheimer et al., 2019). Further south, the extra-tropical North Atlantic decreasing signal converges around the equator with the projected changes in extra-tropical southern swells and the projected changes in tropical waves. As a result, the projected changes in H_s in this region show a small projected decrease that mask the increases in swells propagating from the SO. This behavior enhances during the boreal winter, maximizing the decreases in H_s in the North Atlantic and hence also their contribution beyond the equator, inducing a projected decrease in almost the whole tropical South Atlantic region. Future changes in the extra-tropical North Pacific Ocean do not present a homogenous pattern as in the North Atlantic. First, the spectra at highest latitudes show a general increase in the energy. As we move south, an energy increase associated to westerly swells can be easily identified. This positive change signal evolves to a negative change as we continue moving further from the pole, similarly as it happens in the Southern Hemisphere. During the boreal winter this behavior is maximized, which translates in greater changes in wave

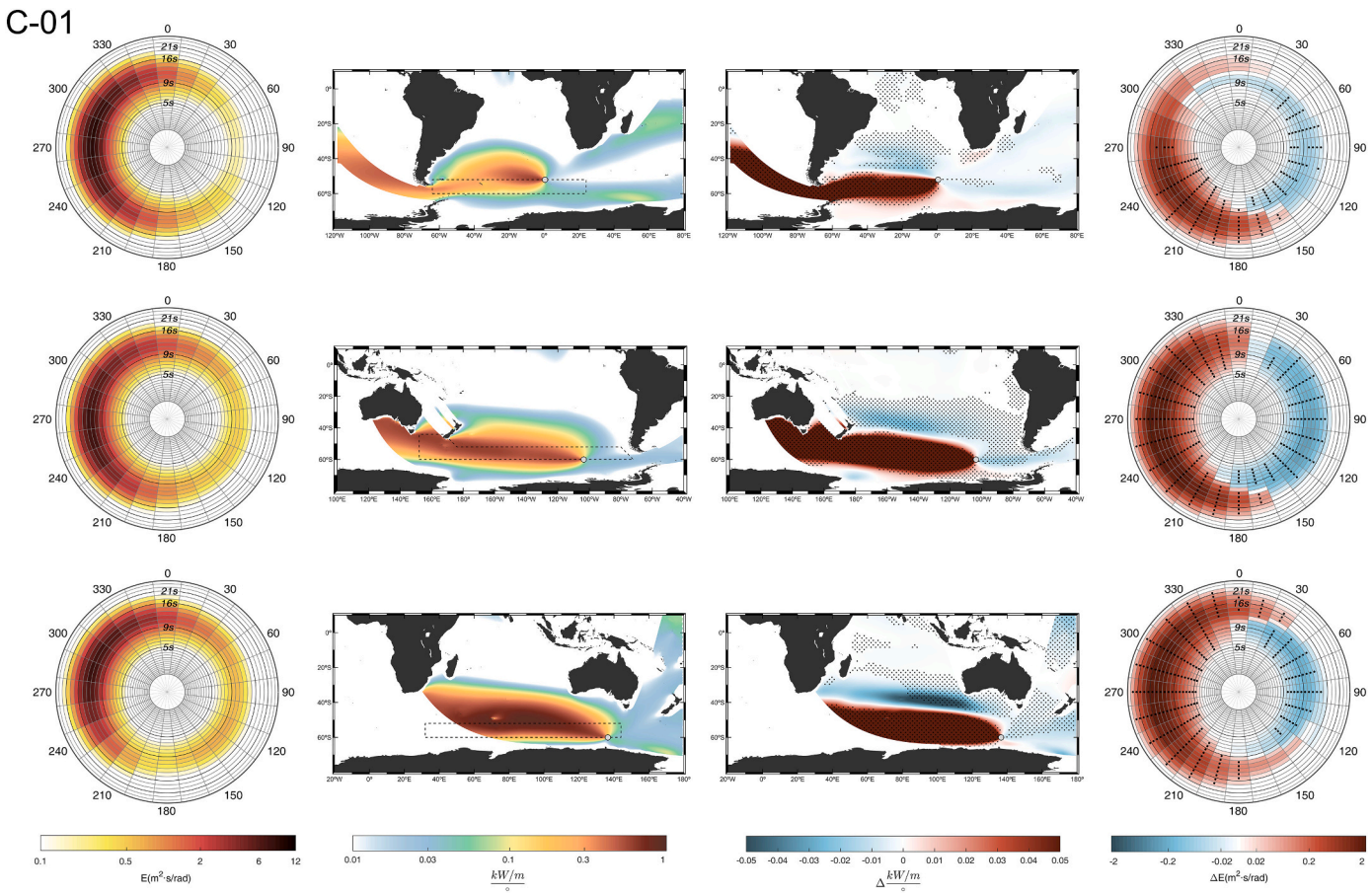

Fig. 9. Analysis of the regional patterns of spectral change in the Southern Ocean. First column: Annual mean wave energy spectrum. Second column: Annual mean effective energy flux propagating toward the target point. The dashed line represents the contour of the cluster. Third column: Ensemble mean change in annual mean effective energy flux propagating toward the target point. Fourth column: Ensemble mean change in the annual mean wave energy spectrum. Stippling indicates robust projected changes.

energy. These high change magnitudes, however, do not appear in H_s since the offset between positive and negative variations within the spectra induces small changes in this parameter. The propagation of these swells to the tropical region causes their change signal to combine with the decrease in tropical waves induced by northeasterly trades and with the projected increase in SO swells. Moreover, during the boreal winter the extra-tropical change signal can travel beyond the equator, also combining with the increases in the waves generated by south-easterly trades. Therefore, the changes in H_s are the result of the integration of those associated to the multiple wave systems propagating in the low Pacific latitudes. For completeness, the contributions from each wave system seasonally vary due to changes in the amount of transported energy. The spectral change pattern in the Indian Ocean is mainly characterized by the combination of the increases expected in SO swells and the changes associated to tropical waves induced by trade winds. Concerning northwestern region, the Indian Ocean area strongly affected by the Monsoon phenomenon, a robust decrease is expected in the wave systems generated by Monsson-induced winds regardless the season.

In order to better understand the estimated spectral changes, we develop an additional analysis which consists in identifying geographic regions with similar spectral change patterns. Then, each region is individually analyzed regarding the propagation behavior of the swells. For example, the sign-of-change boundaries found in the SO and North Pacific require a deeper analysis to be explained, as well as the future behavior of swells generated in the tropical regions by trade winds. The detailed description of the change pattern within these clusters, supported by the ESTELA method, provide a physical basis not only to the spectral changes, but also to the agreed changes in integrated parameters in the different ocean regions.

The resulting classification provides sixteen regional patterns of spectral changes, named from C-01 to C-16 (Fig. 8). The Atlantic, Pacific and Indian oceans are represented by five, seven and three groups, respectively. A unique cluster representing the SO is defined from the merging of the southernmost region of each basin. The final classification separates the spectra characterized by swell increases in the SO from those located further from the pole clearly dominated by a decrease in westerly wave energy. Similarly, other issues such as the high number of clusters in the Pacific, coherent with its multi-modal wave climate, the isolation of the northernmost Atlantic spectra characterized by westerly swell decreases and the transition between the tropical northern and southern Atlantic basins are also distinguished in the obtained groups. Fig. 8 also displays a reference location for each analyzed cluster. The locations are selected as points with a similar spectral change to each cluster centroid given by the k-means algorithm.

We assess the climate change fingerprint on the SO (C-01) by analyzing the spectral changes in each ocean basin (i.e. Atlantic, Pacific and Indian; Fig. 9). The wave climate in this region is characterized by swells propagating eastward all year round (Young, 1999) mostly generated south of 35°S along the roaring forties and furious fifties regions. A robust and clear projected increase is expected in these swells, which agrees with the results found in many studies concerning the future behavior of H_s (e.g. Morim et al., 2018; Oppenheimer et al., 2019). Nevertheless, a clear boundary at approximately 45°S can be observed in every basin, showing a decrease north of that latitude and an increase south of it. This dipole pattern may be related to the expected

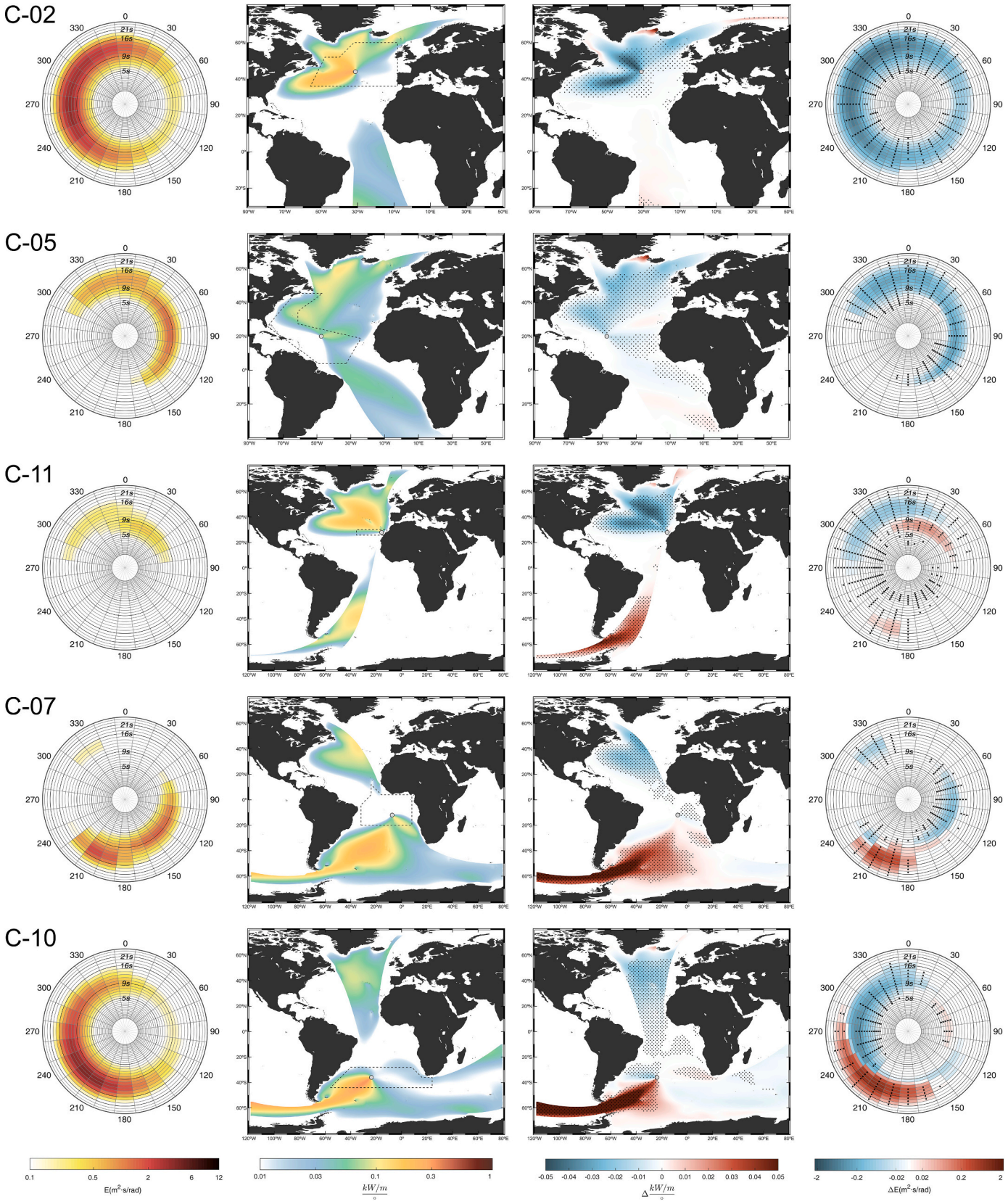

Fig. 10. Same as in Fig. 9 but for the Atlantic Ocean.

poleward shift of the southern extra-tropical storm track (Tamarin-Brodsky and Kaspi, 2017; Yin, 2005) and also favored by the continuous shift of the Southern Annual Mode (SAM) toward its positive phase, which induces a southward shift of subtropical ridge (Fan et al., 2014). In addition, the southern storm track is projected to intensify in a changing climate (Chang et al., 2012; O'Gorman, 2010), which enhances the increasing signal in the southernmost part of the region. These results are consistent and provide an explanation for the projected decrease in H_s north of 35°S found in numerous studies (e.g. Casas-Prat et al., 2018; Hemer et al., 2013; Mori et al., 2013).

Fig. 10 displays the analysis of the clusters from the Atlantic Ocean. C-02 mainly receives energy transported by waves generated by extra-tropical storms crossing the northernmost Atlantic Ocean (Camus et al., 2014; Pérez et al., 2014). Depending on the position of the storm track and the marine ice coverage, waves can be generated in different areas such as the south of Newfoundland, the Labrador Sea and between Iceland and Greenland. These swell systems are characterized by a robust projected decrease regardless of their geographical origin, which is explained by the projected displacement of the storm tracks to higher latitudes and the more frequent atmospheric blocking systems (Lemos et al., 2021a). In addition, results agree and provide confidence in the expected decrease in H_s found by numerous studies in this particular region (e.g. Aarnes et al., 2017; Lemos et al., 2021a). C-05 represents the tropical-north Atlantic region. The energy in this cluster is mainly transported by two systems, waves generated by northeasterly trades and extra-tropical northern swells coming from higher latitudes. Results show a robust decrease in the energy, consistent with the projected decrease expected in H_s. This cluster can also receive energy from waves generated by southeasterly trades and SO swells, although their projected change is negligible in most of the studied region. C-07 pattern shows the future behavior of wind waves in the tropical-south Atlantic Ocean. Projected changes in EF_w show a heterogenous change pattern in trade-induced waves propagating from the southeast. The changes in this swell system and, in general, in waves generated by trade winds are directly linked to the changes in the Hadley Cell (Odériz et al., 2021). In this regard, the expected expansion of this cell globally (Grise and Davis, 2020) affects surface winds fields (Casas-Prat et al., 2018) and provides an explanation to the heterogenous change pattern found in wave energy. Moreover, this cell expansion is also visible in C-05 and C-10 for northern and southern tropical waves, respectively. The south-tropical Atlantic is highly conditioned by the increase expected in SO swells. Therefore, the uncertain increase found in previous studies in this ocean region (e.g. Hemer et al., 2013; Morim et al., 2019) can be explained by the combination of the increase signal from the SO and the uncertain dipole change in tropical waves likely caused by the disagreement of the models in representing the future behavior of the Hadley cell. Most of the energy propagating toward the southernmost cluster of the Atlantic Ocean (C-10) are waves generated by westerly winds south of 40°S within the analyzed cluster and further south in the SO region. The same change signal boundary described in the analysis of the SO that induces positive and negative variations within the spectra can be observed here, providing confidence to the small projected changes in H_s.

The clustering of the Pacific Ocean (Fig. 11) divides the extra-tropical north region in three different clusters. C-09 is located at a very high latitude (60°N) so that the effect of global warming on ice melting has a preponderant role on the homogenous increase found in wave energy due to the significant extension of the generation fetch (Lantuit et al., 2012; Thomson and Rogers, 2014). These changes are remarkably robust in waves from the arctic ocean according to the projected changes in EF_w. In the same vein, C-13, which covers latitudes between 45°N and 55°N, also displays an increase in westerly waves. In addition to the ice melting, the change pattern found can be likely favored by the expected poleward shift of the Pacific storm track (Harvey et al., 2020; Tamarin-Brodsky and Kaspi, 2017). Two main reasons support this statement. First, the analysis of the ensemble mean projected change in ice coverage during boreal winter season (Supplementary Fig. 4) does not sustain the significant increase in waves propagating from the southwest during winter around 180°, nor that the maximum increases are found in those longitudes (Fig. 7). Second, the changes in EF_w show an increase in a proportion of the main generation area, which is not affected by a major decrease in ice coverage. Nevertheless, results should be taken with caution as there exists great uncertainty in the projected changes in EF_w in this region, likely indicating discrepancies between models concerning the definition of the storm tracks and their future behavior (Priestley et al., 2020), as well as on the ice melting projection (Supplementary Fig. 4). As we move south, the decrease in wave energy dominates the region north of 30°N. This issue is represented by C-03, whose change pattern shows a homogenous decrease both in extra-tropical waves and in tropical waves generated by northeasterly trades; the latter being consistent with previous studies that analyzed the future behavior of surface winds (Casas-Prat et al., 2018). As previously explained, wave climate in C-06, C-12 and C-16 is characterized by multiple wave systems whose different contribution is highly seasonal (Fig. 5, Supplementary Fig. 2). Concerning C-16, it is mainly reached by five wave systems: southern waves generated south of 30°S, waves induced by southeasterly trades, waves generated by northeasterly trades, waves generated by the Californian low level coastal jet and northern extra-tropical waves (Jiang and Mu, 2019). The change in wave energy from the first two systems evidence a robust increasing signal. Note that the latter is consistent with the expected intensification in southeasterly trades found in previous studies (Timmermann et al., 2010). The combination of both change signals results in a projected increase in H_s consistent with the community agreement (Oppenheimer et al., 2019). Moreover, a poleward shift can still be discerned from the spectrum and EF_w changes for both wave systems. The decreasing signal associated with the other three described systems slightly contributes to reduce the projected change in H_s. In C-12 the contribution of the increasing signal from the extra-tropical southern swells reduces due to the presence of Australia and the importance of trade-induced waves enhances. Thus, the most important wave system are swells generated by northeasterly trades. In addition, this cluster receives energy from southeasterly tropical swells and extra-tropical waves form both hemispheres. Consistently with previous clusters, changes in EF_w show a robust decrease in northeasterly and northern extra-tropical waves and an increase in southeasterly swells. Similarly, C-06 is also highly affected by southeasterly swells although its southern latitude makes it also reached by a high amount of energy from the SO. The change signals agree with those already discussed for previous clusters. Finally, C-14 is located south of 40°S so that it mainly receives energy transported by waves generated by southern westerly winds. As it was observed in the SO (Fig. 9) and in the southernmost cluster of the Atlantic Ocean (Fig. 10), a robust transition from positive to negative changes appears around 45°S.

Fig. 12 shows the analysis of the three clusters in the Indian Ocean. Wave climate in C-08 is mainly represented by three wave systems: waves generated by southeasterly trade winds, waves generated in the extra-tropical southern region and waves generated by monsoon-induced winds. Concerning the first system, the projected changes in EF_w show a dipole pattern likely indicating a poleward shift. This issue can also be observed in C-15, both cases characterized by a significant uncertainty. In addition, the expected increase in energy from SO swells and the projected decrease in monsoon waves also reach the analyzed cluster. Apart from trade-induced waves, C-15 is affected by westerly swells generated south of 35°S. In this regard, as this cluster extends between 25°S and 35°S, the decreases expected in westerly waves north of 45°S dominate the change signal within the cluster, causing an expected decrease in H_s. Projected changes in C-04 are already described as it is mostly affected by southern westerly swells.

5. Concluding remarks

The present study assesses the projected changes in wave climate

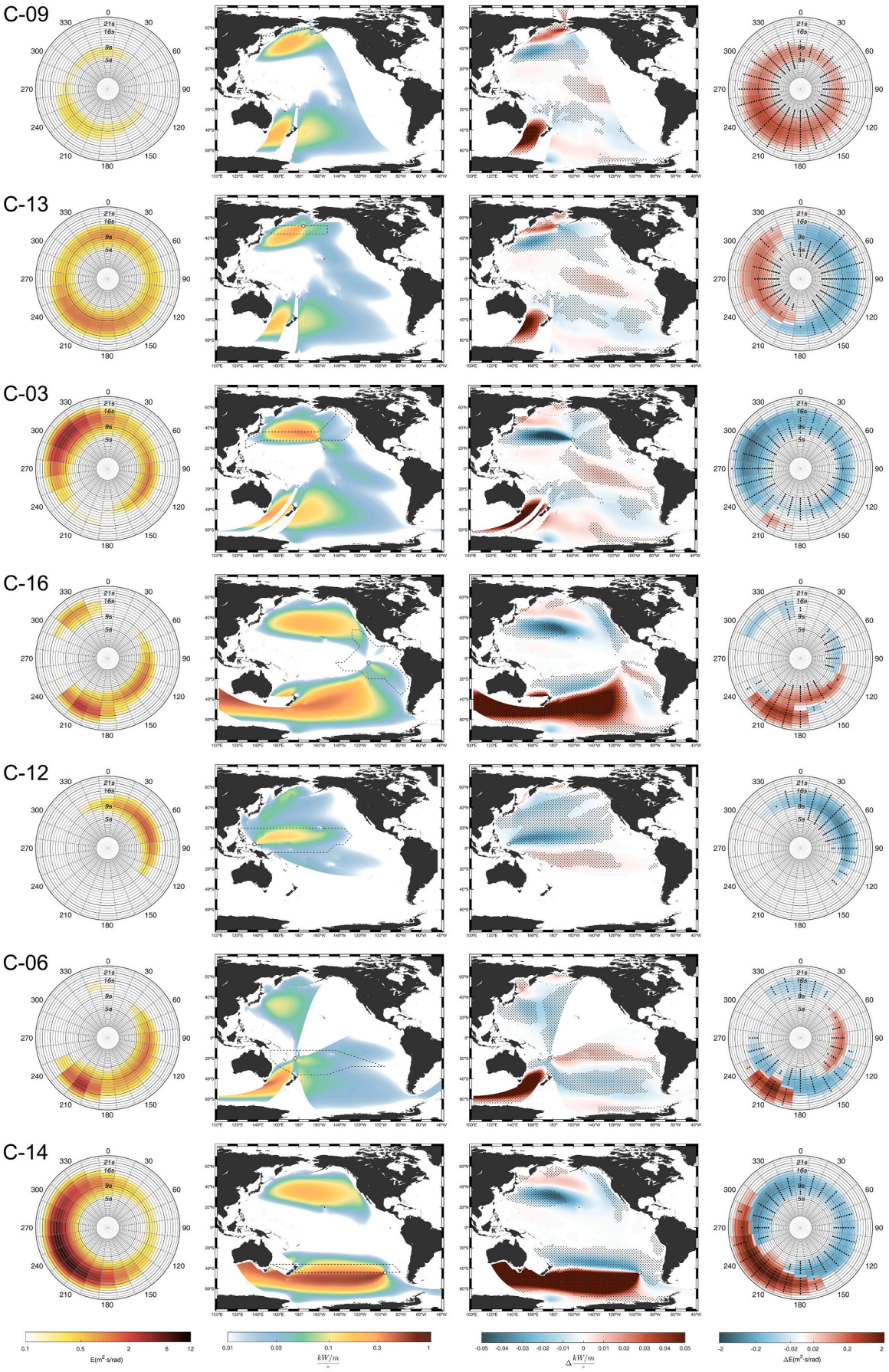

Fig. 11. Same as in Fig. 9 but for the Pacific Ocean.

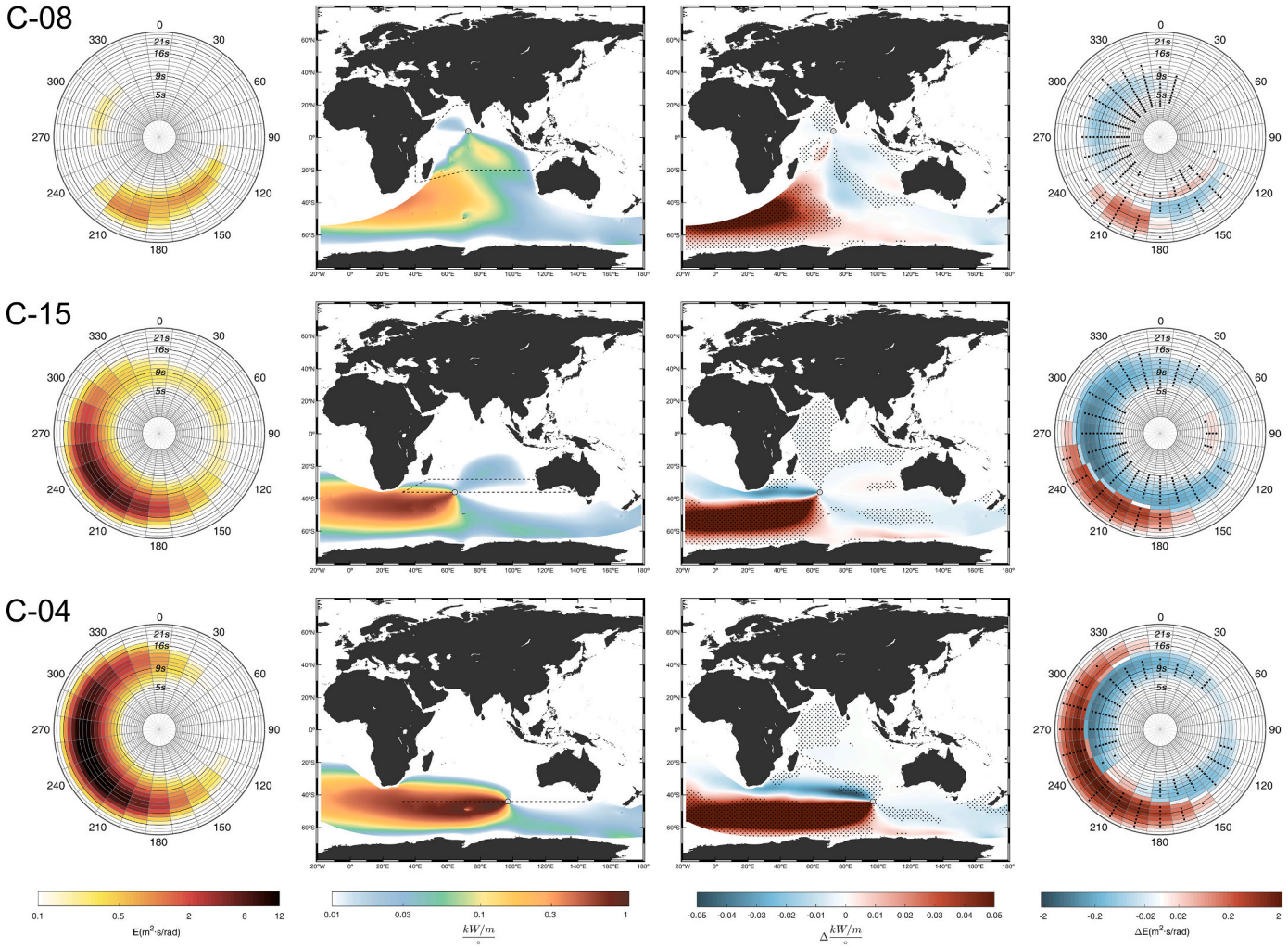

Fig. 12. Same as in Fig. 9 but for the Indian Ocean.

globally from a novel perspective based on the use of directional spectra. Seven GCM-based wave climate members (Table 1) are analyzed to estimate mean ensemble changes and related uncertainty by the end of the century under the RCP8.5 high-emissions scenario. The skill of the models to reproduce the historical wave climatology is assessed by comparison against a reference hindcast (Supplementary Fig. 1). We find low-magnitude biases, which provides confidence in the representation of the wave climatology. However, further research is needed to develop a methodology to correct the intrinsic bias of directional spectra and provide more accurate results.

The projected changes in directional spectra provide much more information about the future change in wave climate than an analysis approached by assessing the variations in integrated parameters only, such as significant wave height. The spectral changes evidence the propagation of the change signal associated with each wave system from the generation area. Hence, the assessment of the spectral change at a certain location offers a clear view of the combination of all the signals, each of them characterized by a magnitude and sign of change. On this basis, the use of integrated parameter disguises most of this information as it cannot discern the different contributing change signals, nor their individual characteristics.

To complete the spectral analysis, we cluster the annual mean spectral changes. Sixteen groups distributed through ocean basins with a similar spectral change pattern are found (Fig. 8). Then, we explore the propagation scheme of the main wave systems arriving at the representing point from each group to assess the changes in the transported energy flux and their influence in the change patterns found. The individual analysis of each cluster (Figs. 9 to 12) together with the overview provided by the annual (Fig. 6) and seasonal (Fig. 7) global changes, makes us reach solid conclusions about the expected change in the main swell systems propagating across the oceans.

Results show a robust increase in the energy transported by westerly swells generated south of 45°S. This change signal propagates and is noticeable in both hemispheres, reaching latitudes higher than 30°N in the Pacific and Atlantic oceans, mainly during the austral winter. Around 45°S, a clear transition to a decreasing change signal in westerly swells likely caused by a poleward shift of the southern storm track can be observed, inducing a projected decrease in significant wave height north of the mentioned latitude. The projected behavior in the northern storm track is significantly different between the Atlantic and the Pacific oceans. While the Atlantic Ocean shows a homogenous decrease regardless of the generation area, the Pacific Ocean shows three different spectral change patterns. In the Pacific, the combined effect of the ice melting in high latitudes and the expected change in the storm track causes a transition from a projected increase to a decrease in northern westerly waves, similarly to the southern extra-tropical region.

The complex interaction between different wave systems in the tropical latitudes can only be assessed from a spectral perspective. The change pattern can also vary within the year mainly depending on the contribution of the change signal associated with extra-tropical wave systems (Fig. 7). The projected change in the energy transported by waves generated by trade winds varies depending on the ocean basin.

The Pacific and North Atlantic basins show the clearest change pattern in trade waves, projecting a decrease in northeasterly waves in both basins and an increase in southeasterly waves in the Pacific. The poleward shift expected in trade winds due to the expansion of the Hadley cell dominates the trade wave systems in the South Atlantic and Indian basins, therefore inducing a dipole change pattern and precluding determination of a clear change signal associated with the wave energy.

The assessment of projected changes in directional spectra provides a solid basis to the future variations in integrated wave parameters. For example, results show that the decreases in significant wave height projected in the North Atlantic Ocean are mainly caused by a projected decrease in both extra-tropical waves and in northeasterly trade waves. Also, the agreed increase in H_s in the tropical eastern Pacific is significantly influenced by the increase in Southern Ocean swells together with the increases in southeasterly trade waves. Further research on physical processes such as the ice melting in high latitudes, changes in storm tracks and shifts in the main wind systems may elucidate the causes of the found projected changes in wave spectra. In addition, the skill of the climate models to reproduce these physical processes should also be analyzed as it might be a major source of uncertainty. It is relevant to point out that the number of partitions and the reconstruction scheme used in this study imply some limitations that should also be considered when interpreting the results. The use of three partitions to reconstruct the directional spectrum may smooth the energy content of secondary wave systems in ocean areas recurrently reached by more than two swells simultaneously, mainly in the tropical region. Consistently, the projected change in the energy carried by these wave systems is also expected to be smoothed, although not varying the sign of change. In addition, the reconstructed spectrum is an approximation of the full spectrum based on a theoretical shape. Although the validation shows a good representation of the full spectrum using a JONSWAP shape with a standard peak enhancement parameter value of 3.3 (Fig. 2), further research is needed on the evaluation of the most accurate spectral shape to reconstruct each wave system.

The information provided by the spectral approach can be relevant in coastal impact assessment (i.e. flooding and erosion). Identifying changes in different wave systems and including them in impact studies, rather than integrated parameters only, could provide different results. A detail individual analysis of the projected changes in each wave system may give a more realistic prospect of the impacts the wave climate changes would have in a target coastal stretch, not masking, as it happens with integrated parameters, relevant changes in key variables such as period and direction.

To conclude, this study aims to entail a solid argument to assess the projected changes in wave climate through a novel perspective based on spectral information, opening the door to the next logical step along this new approach, namely developing studies based on full directional spectra and not restricted to the limitations inherent to reconstructed spectra.

Declaration of Competing Interest

The authors declare that they have no known competing financial interests or personal relationships that could have appeared to influence the work reported in this paper.

Acknowledgments

H.L. acknowledges the financial support from the Spanish Ministry of Universities (Grant FPU17/06203). This study is supported by the grant EXCEED (RTI2018-096449-B-I00) funded by MCIN/AEI/10.13039/501100011033 and by the European Commission through the project CoCliCo (101003598, Call: H2020-LC-CLA-2020-2).

Appendix A. Supplementary data

Supplementary data to this article can be found online at https://doi.org/10.1016/j.gloplacha.2022.103820.

References

Aarnes, O.J., Reistad, M., Breivik, Ø., Bitner-Gregersen, E., Ingolf Eide, L., Gramstad, O., Vanem, E., 2017. Projected changes in significant wave height toward the end of the 21st century: Northeast Atlantic. J. Geophys. Res. Oceans 122 (4), 3394–3403. https://doi.org/10.1002/2016JC012521.

Alvarez-Cuesta, M., Toimil, A., Losada, I.J., 2021a. Modelling long-term shoreline evolution in highly anthropized coastal areas. Part 1: model description and validation. Coast. Eng. 169 (July), 103960 https://doi.org/10.1016/j.coastaleng.2021.103960.

Alvarez-Cuesta, M., Toimil, A., Losada, I.J., 2021b. Reprint of: modelling long-term shoreline evolution in highly anthropized coastal areas. Part 2: assessing the response to climate change. Coast. Eng. 169, 103985 https://doi.org/10.1016/j.coastaleng.2021.103985.

Amores, A., Marcos, M., 2020. Ocean swells along the global coastlines and their climate projections for the twenty-first century. J. Clim. 33 (1), 185–199. https://doi.org/10.1175/JCLI-D-19-0216.1.

Arthur, D., Vassilvitskii, S., 2007. K-means++: The advantages of careful seeding. In: Proceedings of the Annual ACM-SIAM Symposium on Discrete Algorithms, 07-09-Janu, pp. 1027–1035.

Benoit, M., 1992. Practical comparative performance survey of methods used for estimating directional wave spectra from heave-pitch-roll data. Coast. Eng. 62–75.

Boukhanovsky, A.V., Lopatoukhin, L.J., Guedes Soares, C., 2007. Spectral wave climate of the North Sea. Appl. Ocean Res. 29 (3), 146–154. https://doi.org/10.1016/j.apor.2007.08.004.

Camus, Paula, Mendez, F.J., Medina, R., Cofiño, A.S., 2011. Analysis of clustering and selection algorithms for the study of multivariate wave climate. Coast. Eng. 58 (6), 453–462. https://doi.org/10.1016/j.coastaleng.2011.02.003.

Camus, P., Menéndez, M., Méndez, F.J., Izaguirre, C., Espejo, A., Cánovas, V., Medina, R., 2014. A weather-type statistical downscaling framework for ocean wave climate. J. Geophys. Res. Oceans 119 (11), 7389–7405. https://doi.org/10.1002/2014JC010141.

Camus, P., Losada, I.J., Izaguirre, C., Espejo, A., Menendez, M., Perez, J., 2017. Statistical wave climate projections for coastal impact Earth ' s Future. Earth's Future. https://doi.org/10.1002/eft2.234.

Casas-Prat, M., Wang, X.L., Swart, N., 2018. CMIP5-based global wave climate projections including the entire Arctic Ocean. Ocean Model 123 (April 2017), 66–85. https://doi.org/10.1016/j.ocemod.2017.12.003.

Chang, E.K.M., Guo, Y., Xia, X., 2012. CMIP5 multimodel ensemble projection of storm track change under global warming. J. Geophys. Res.-Atmos. 117 (23), 1–19. https://doi.org/10.1029/2012JD018578.

Collins, M., Knutti, R., Arblaster, J., Dufresne, J.-L., Fichefet, T., Friedlingstein, P., Wehner, M., 2013. Long-term climate change: Projections, commitments and irreversibility. In: Climate Change 2013: the Physical Science Basis: Working Group I Contribution to the Fifth Assessment Report of the Intergovernmental Panel on Climate Change. https://doi.org/10.1017/CBO9781107415324.024.

Cubasch, U., Wuebbles, D., Chen, D., Facchini, M.C., Frame, D., Mahowald, N., Winther, J.-G., 2013. Introduction. In: Stocker, T.F., Quin, D., Plattner, G.-K., Tignor, M., Allen, S.K., Boschung, J., Midgley, P.M. (Eds.), Climate Change 2013: The Physical Science Basis. Contribution of Working Group I to the Fifth Assessment Report of the Intergovenermnetal Panel on Climate Change. https://doi.org/10.2753/JES1097-203X330403.

Dima, I.M., Wallace, J.M., 2003. On the seasonality of the Hadley Cell. J. Atmos. Sci. 60 (12), 1522–1527. https://doi.org/10.1175/1520-0469(2003)060<1522:OTSOTH>2.0.CO;2.

Donelan, M.A., Hamilton, J., Hui, W.H., 1985. Directional spectra of wind-generated ocean waves. Philos. Trans. Royal Soc. Lond. Ser. A Math. Phys. Sci. 315, 509–562. https://doi.org/10.1098/rsta.1985.0054.

Echevarria, E.R., Hemer, M.A., Holbrook, N.J., 2019. Seasonal variability of the global spectral wind wave climate. J. Geophys. Res. Oceans 124 (4), 2924–2939. https://doi.org/10.1029/2018JC014620.

Echevarria, E.R., Hemer, M.A., Holbrook, N.J., Marshall, A.G., 2020. Influence of the Pacific-South American modes on the global spectral wind-wave climate. J. Geophys. Res. Oceans 125 (8), 1–16. https://doi.org/10.1029/2020JC016354.

Espejo, A., Camus, P., Losada, I.J., Méndez, F.J., 2014. Spectral ocean wave climate variability based on atmospheric circulation patterns. J. Phys. Oceanogr. 44 (8), 2139–2152. https://doi.org/10.1175/JPO-D-13-0276.1.

Fan, Y., Held, I.M., Lin, S.J., Wang, X.L., 2013. Ocean warming effect on surface gravity wave climate change for the end of the twenty-first century. J. Clim. 26 (16), 6046–6066. https://doi.org/10.1175/JCLI-D-12-00410.1.

Fan, Y., Lin, S.J., Griffies, S.M., Hemer, M.A., 2014. Simulated global swell and wind-sea climate and their responses to anthropogenic climate change at the end of the twenty-first century. J. Clim. 27 (10), 3516–3536. https://doi.org/10.1175/JCLI-D-13-00198.1.

Flato, G., Marotzke, J., Abiodun, B., Braconnot, P., Chou, S.C., Collins, W., Rummukainen, M., 2013. Evaluation of climate models. In: Stocker, T.F., Quin, D., Plattner, G.-K., Tignor, M., Allen, S.K., Boschung, J., Midgley, P.M. (Eds.), Climate Change 2013: The Physical Science Basis. Contribution of Working Group I to the Fifth Assessment Report of the Intergovenermnetal Panel on Climate Change.

Goda, Y., 2010. Random seas and design of maritime structures. In: Advanced Series on Ocean Engineering, vol. 33.
Grise, K.M., Davis, S.M., 2020. Hadley cell expansion in CMIP6 models. Atmos. Chem. Phys. 20, 5249–5268. https://doi.org/10.5194/acp-20-5249-2020.
Hanson, J.L., Phillips, O.M., 2001. Automated analysis of ocean surface directional wave spectra. J. Atmos. Ocean. Technol. 18 (2), 277–293. https://doi.org/10.1175/1520-0426(2001)018<0277:AAOOSD>2.0.CO;2.
Harvey, B.J., Cook, P., Shaffrey, L.C., Schiemann, R., 2020. The response of the Northern Hemisphere storm tracks and jet streams to climate change in the CMIP3, CMIP5, and CMIP6 climate models. J. Geophys. Res.-Atmos. 125 (23), 1–10. https://doi.org/10.1029/2020JD032701.
Hasselmann, K., Barnett, T.P., Bouws, E., Carlson, H., Cartwright, D.E., Eake, K., Walden, H., 1973. Measurements of Wind-Wave Growth and Swell Decay during the Joint North Sea Wave Project (JONSWAP).
Hemer, M.A., McInnes, K.L., Ranasinghe, R., 2012. Climate and variability bias adjustment of climate model-derived winds for a southeast Australian dynamical wave model. Ocean Dyn. 62 (1), 87–104. https://doi.org/10.1007/s10236-011-0486-4.
Hemer, M.A., Fan, Y., Mori, N., Semedo, A., Wang, X.L., 2013. Projected changes in wave climate from a multi-model ensemble. Nat. Clim. Chang. 3 (5), 471–476. https://doi.org/10.1038/nclimate1791.
Holthuijsen, L.H., 2007. Waves in oceanic and coastal waters. In: Waves in Oceanic and Coastal Waters, vol. 9780521860284. https://doi.org/10.1017/CBO9780511618536.
Jiang, H., Mu, L., 2019. Wave climate from spectra and its connections with local and remote wind climate. J. Phys. Oceanogr. 49 (2), 543–559. https://doi.org/10.1175/JPO-D-18-0149.1.
Kaufman, L., Rousseeuw, P.J., 2009. Finding Groups in Data: An Introduction to Cluster Analysis, vol. 344. John Wiley & Sons.
Lantuit, H., Overduin, P.P., Couture, N., Wetterich, S., Aré, F., Atkinson, D., Vasiliev, A., 2012. The Arctic coastal dynamics database: a new classification scheme and statistics on Arctic Permafrost coastlines. Estuar. Coasts. https://doi.org/10.1007/s12237-010-9362-6.
Lemos, G., Semedo, A., Dobrynin, M., Behrens, A., Staneva, J., Bidlot, J.R., Miranda, P.M. A., 2019. Mid-twenty-first century global wave climate projections: results from a dynamic CMIP5 based ensemble. Glob. Planet. Chang. 172 (July 2018), 69–87. https://doi.org/10.1016/j.gloplacha.2018.09.011.
Lemos, G., Menendez, M., Semedo, A., Camus, P., Hemer, M., Dobrynin, M., Miranda, P. M.A., 2020. On the need of bias correction methods for wave climate projections. Glob. Planet. Chang. 186 (August 2019), 103109. https://doi.org/10.1016/j.gloplacha.2019.103109.
Lemos, G., Menendez, M., Semedo, A., Miranda, P.M.A., Hemer, M., 2021a. On the decreases in North Atlantic significant wave heights from climate projections. Clim. Dyn. 0123456789 https://doi.org/10.1007/s00382-021-05807-8.
Lemos, G., Semedo, A., Hemer, M., Menendez, M., Miranda, P.M.A., 2021b. Remote climate change propagation across the oceans – the directional swell signature. Environ. Res. Lett. https://doi.org/10.1088/1748-9326/ac046b. Retrieved from.
Lloyd, S.P., 1982. Least squares quantization in PCM. IEEE Trans. Inf. Theory 28 (2), 129–137. https://doi.org/10.1109/TIT.1982.1056489.
Lobeto, H., Menendez, M., Losada, I.J., 2021a. Future behavior of wind wave extremes due to climate change. Sci. Rep. 11 (1), 1–12. https://doi.org/10.1038/s41598-021-86524-4.
Lobeto, H., Menendez, M., Losada, I.J., 2021b. Projections of directional spectra help to unravel the future behavior of wind waves. Front. Mar. Sci. 8 (May) https://doi.org/10.3389/fmars.2021.655490.
Longuet-Higgins, M.S., Cartwright, D.E., Smith, N.D., 1963. Observations of the directional spectrum of sea waves using the motions of a floating buoy. Ocean Wave Spectra 111–136.
Lucio, D., Tomás, A., Lara, J.L., Camus, P., Losada, I.J., 2020. Stochastic modeling of long-term wave climate based on weather patterns for coastal structures applications. Coast. Eng. 161 (July), 103771 https://doi.org/10.1016/j.coastaleng.2020.103771.
Maraun, D., Shepherd, T.G., Widmann, M., Zappa, G., Walton, D., Gutiérrez, J.M., Mearns, L.O., 2017. Towards process-informed bias correction of climate change simulations. Nat. Clim. Chang. 7 (11), 764–773. https://doi.org/10.1038/nclimate3418.
Mentaschi, L., Vousdoukas, M.I., Voukouvalas, E., Dosio, A., Feyen, L., 2017. Global Changes of Extreme Coastal Wave Energy Fluxes Triggered by Intensified Teleconnection Patterns, pp. 2416–2426. https://doi.org/10.1002/2016GL072488.
Mitsuyasu, H., Tasai, F., Suhara, T., Mizuno, S., Ohkusu, M., Honda, T., Rikiishi, K., 1975. Observation of the directional spectrum of ocean waves using a cloverleaf buoy. Phys. Oceanogr. 5, 750–760. Retrieved from http://www.ghbook.ir/index.php?name=مجموعه مقالات دومین مم انديشی سراسری رسانه تلويزيون و&option=com_dbook&task=readonline&book_id=13629&page=108&chkhashk=03C706812F&Itemid=218&lang=fa&tmpl=component.
Mori, N., Shimura, T., Yasuda, T., Mase, H., 2013. Multi-model climate projections of ocean surface variables under different climate scenarios-Future change of waves, sea level and wind. Ocean Eng. 71, 122–129. https://doi.org/10.1016/j.oceaneng.2013.02.016.
Morim, J., Hemer, M., Cartwright, N., Strauss, D., Andutta, F., 2018. On the concordance of 21st century wind-wave climate projections. Glob. Planet. Chang. 167 (May), 160–171. https://doi.org/10.1016/j.gloplacha.2018.05.005.
Morim, J., Hemer, M., Wang, X.L., Cartwright, N., Trenham, C., Semedo, A., Andutta, F., 2019. Robustness and uncertainties in global multivariate wind-wave climate projections. Nat. Clim. Chang. 9 (9), 711–718. https://doi.org/10.1038/s41558-019-0542-5.
Morim, J., Trenham, C., Hemer, M., Wang, X.L., Mori, N., Casas-Prat, M., Erikson, L., 2020. A global ensemble of ocean wave climate projections from CMIP5-driven models. Sci. Data 7 (1), 1–10. https://doi.org/10.1038/s41597-020-0446-2.
Odériz, I., Silva, R., Mortlock, T.R., Mori, N., Shimura, T., Webb, A., Villers, S., 2021. Natural variability and warming signals in global ocean wave climates. Geophys. Res. Lett. 1–12 https://doi.org/10.1029/2021gl093622.
O'Gorman, P.A., 2010. Understanding the varied response of the extratropical storm tracks to climate change. Proc. Natl. Acad. Sci. U. S. A. 107 (45), 19176–19180. https://doi.org/10.1073/pnas.1011547107.
Onorato, M., Osborne, A.R., Serio, M., Bertone, S., 2001. Freak waves in random oceanic sea states. Phys. Rev. Lett. 86 (25), 5831–5834. https://doi.org/10.1103/PhysRevLett.86.5831.
Oppenheimer, M., Glavovic, B., Hinkel, J., van de Wal, R., Magnan, A.K., Abd-Elgawad, A., Sebesvari, Z., 2019. Sea level rise and implications for low lying Islands, coasts and communities. In: IPCC Special Report on the Ocean and Cryosphere in a Changing Climate.
Pérez, J., Méndez, F.J., Menéndez, M., Losada, I.J., 2014. ESTELA: a method for evaluating the source and travel time of the wave energy reaching a local area. Ocean Dyn. 64 (8), 1181–1191. https://doi.org/10.1007/s10236-014-0740-7.
Perez, J., Menendez, M., Camus, P., Mendez, F.J., Losada, I.J., 2015. Statistical multi-model climate projections of surface ocean waves in Europe. Ocean Model 96, 161–170. https://doi.org/10.1016/j.ocemod.2015.06.001.
Pierson Jr., W.J., Tuttell, J.J., Woolley, J.A., 1952. The theory of the refraction of a short crested gaussian sea surface with application to the northern New Jersey Coast. In: 3rd Conf. Coastal Engineering, pp. 86–108. https://doi.org/10.9753/icce.v3.8.
Portilla, J., Ocampo-Torres, F.J., Monbaliu, J., 2009. Spectral partitioning and identification of wind sea and swell. J. Atmos. Ocean. Technol. 26 (1), 107–122. https://doi.org/10.1175/2008JTECHO609.1.
Portilla-Yandún, J., 2018. The global signature of ocean wave spectra. Geophys. Res. Lett. 45 (1), 267–276. https://doi.org/10.1002/2017GL076431.
Portilla-Yandún, J., Cavaleri, L., Van Vledder, G.P., 2015. Wave spectra partitioning and long term statistical distribution. Ocean Model 96, 148–160. https://doi.org/10.1016/j.ocemod.2015.06.008.
Portilla-Yandún, J., Barbariol, F., Benetazzo, A., Cavaleri, L., 2019. On the statistical analysis of ocean wave directional spectra. Ocean Eng. 189 (August), 106361 https://doi.org/10.1016/j.oceaneng.2019.106361.
Priestley, M.D.K., Ackerley, D., Catto, J.L., Hodges, K.I., McDonald, R.E., Lee, R.W., 2020. An overview of the extratropical storm tracks in CMIP6 historical simulations. J. Clim. 33 (15), 6315–6343. https://doi.org/10.1175/JCLI-D-19-0928.1.
Reguero, B.G., Losada, I.J., Méndez, F.J., 2019. A recent increase in global wave power as a consequence of oceanic warming. Nat. Commun. 10 (1) https://doi.org/10.1038/s41467-018-08066-0.
Rueda-bayona, J.G., Ph, D., Guzmán, A., Ph, D., Asce, M., José, J., Ph, D., 2020. Selection of JONSWAP spectra parameters during water-depth and sea-state transitions, 146 (6), 1–13. https://doi.org/10.1061/(ASCE)WW.1943-5460.0000601.
Semedo, A., SušElj, K., Rutgersson, A., Sterl, A., 2011. A global view on the wind sea and swell climate and variability from ERA-40. J. Clim. 24 (5), 1461–1479. https://doi.org/10.1175/2010JCLI3718.1.
Semedo, A., Weisse, R., Behrens, A., Sterl, A., Bengtsson, L., Günther, H., 2013. Projection of global wave climate change toward the end of the twenty-first century. J. Clim. 26 (21), 8269–8288. https://doi.org/10.1175/JCLI-D-12-00658.1.
Shimura, T., Mori, N., 2019. High-resolution wave climate hindcast around Japan and its spectral representation. Coast. Eng. 151 (May), 1–9. https://doi.org/10.1016/j.coastaleng.2019.04.013.
Snarey, M., Terrett, N.K., Willett, P., Wilton, D.J., 1997. Comparison of algorithms for dissimilarity-based compound selection. J. Mol. Graph. Model. 15 (6), 372–385. https://doi.org/10.1016/S1093-3263(98)00008-4.
Tamarin-Brodsky, T., Kaspi, Y., 2017. Enhanced poleward propagation of storms under climate change. Nat. Geosci. 10 (12), 908–913. https://doi.org/10.1038/s41561-017-0001-8.
Tebaldi, C., Arblaster, J.M., Knutti, R., 2011. Mapping model agreement on future climate projections. Geophys. Res. Lett. 38 (23), 1–5. https://doi.org/10.1029/2011GL049863.
Thomson, J., Rogers, W.E., 2014. Swell and sea in the emerging Arctic Ocean. Geophys. Res. Lett. 41 (9), 3136–3140. https://doi.org/10.1002/2014GL059983.
Timmermann, A., McGregor, S., Jin, F.F., 2010. Wind effects on past and future regional sea level trends in the southern Indo-Pacific. J. Clim. 23 (16), 4429–4437. https://doi.org/10.1175/2010JCLI3519.1.
Toimil, A., Camus, P., Losada, I.J., Alvarez-Cuesta, M., 2021. Visualising the uncertainty cascade in multi-ensemble probabilistic coastal erosion projections. Front. Mar. Sci. 8 (June), 1–19. https://doi.org/10.3389/fmars.2021.683535.
Tolman, H.L., 2014. User Manual and System Documentation of WAVEWATCH III.
Tracy, B., Devaliere, E., Hanson, J., Nicolini, T., Tolman, H., 2007. Wind Sea and swell delineation for numerical wave modeling. In: 10th International Workshop on Wave Hindcasting and Forecasting Coastal Hazard Symposium. Retrieved from papers2://publication/uuid/BDC84DF4-52C0-4FB7-AC88-5FBEDCE68D4F.
Usace, 1984. Shore Protection Manual, Waterways Experiment Station, Corps of Engineers. Department of the Army, Waterways Experiment Station, p. 1, II.
Wang, Y., 2014. Calculating crest statistics of shallow water nonlinear waves based on standard spectra and measured data at the Poseidon platform. Ocean Eng. 87, 16–24. https://doi.org/10.1016/j.oceaneng.2014.05.012.
Wang, X.L., Feng, Y., Swail, V.R., 2014. Changes in global ocean wave heights as projected using multimodel CMIP5 simulations. Geophys. Res. Lett. 41 (3), 1026–1034. https://doi.org/10.1002/2013GL058650.

Whittaker, C.N., Raby, A.C., Fitzgerald, C.J., Taylor, P.H., 2016. The average shape of large waves in the coastal zone. Coast. Eng. 114, 253–264. https://doi.org/10.1016/j.coastaleng.2016.04.009.

Yin, J.H., 2005. A consistent poleward shift of the storm tracks in simulations of 21st century climate. Geophys. Res. Lett. 32 (18), 1–4. https://doi.org/10.1029/2005GL023684.

Young, I.R., 1999. Seasonal variability of the global ocean wind and wave climate. Int. J. Climatol. 19 (9), 931–950. https://doi.org/10.1002/(SICI)1097-0088(199907)19:9<931::AID-JOC412>3.0.CO;2-O.